JOURNAL OF AIRCRAFT
Vol. 41, No. 6, November–December 2004

Influence of Nonlinear Elastomer on Isolated Lag Dynamics and Rotor/Fuselage Aeromechanical Stability

G. Pohit,* C. Venkatesan,† and A. K. Mallik‡
Indian Institute of Technology Kanpur, Kanpur 208016, India

This paper presents a study on the effect of nonlinearities of an elastomeric bearing on isolated lag dynamics and coupled rotor/fuselage ground resonance stability of an idealized bearingless rotor blade. The rotor blade is modeled as an elastic beam with a nonlinear elastomer and a rigid torque tube. First, amplitudedependent natural frequency of the blade in lag mode is analyzed using numerical perturbation technique. Then the problem of amplitude-dependent stability of the coupled rotor/fuselage system under ground resonance condition is investigated. The stability of the system is analyzed by two approaches, namely, 1) by eigenanalysis of the linearized equations and 2) by response of the nonlinear system to an initial disturbance by time integration. The results of the eigenanalysis indicate that the effect of amplitude seems to be more dominant on the progressive lag mode damping than on regressive lag mode damping. It is also observed that so far as the stability in ground resonance is concerned there exist optimum locations for the attachment of both the elastomer and torque tube. Results of the time-domain analysis of the nonlinear equations indicate clearly that the stability of the system is dependent on the magnitude of initial disturbance.

Nomenclature

$\hat{A}_i$	=	amplitude of motion
$\bar{C}$	=	nondimensional damping, $C^*\hat{\Psi}_1^2$
C_{eq}, K_{eq}	=	equivalent damping and stiffness
C_x, C_y	=	nondimensional damping coefficients of support in roll and pitch mode
C^*	=	nondimensional damping coefficient of the elastomer, $C_{\text{eq}}/m\Omega L$
D_0	=	amplitude of excitation of elastomer
F	=	coulomb damping coefficient
K', K''	=	amplitude-dependent inphase and quadrature stiffnesses of the elastomer
L	=	blade length
m	=	mass per unit length of the blade
h_1	=	hysteretic damping coefficient
$\bar{h}$	=	height of rotor above fuselage c.g.
I_x, I_y	=	nondimensional rotary inertia in roll and pitch mode, respectively
K_x, K_y	=	nondimensional stiffnesses of the support in roll and pitch mode
K_1, K_3, K_5, K_7	=	stiffness parameters of spring
M, C, K	=	mass, damping, and stiffness matrices
$\hat{M}$, $\hat{C}$, $\hat{K}$	=	mass, damping, and stiffness matrices in time-domain analysis
s_j	=	complex eignvalues, $s_j = \sigma_j \pm i\omega_j$
$\bar{u}$	=	axial displacement of the blade
v	=	nondimensional in-plane displacement
v_k	=	nondimensional in-plane displacement of the k-th blade
$\bar{v}$	=	in-plane displacement of the blade
z_i	=	ith lag mode
z_{ic}, z_{is}	=	cyclic lag coordinates in ith mode
z_{ik}	=	generalized coordinate of ith lag mode of kth blade
Z_p, Z_r	=	progressive and regressive lag mode
Δ_i	=	spring deformation
ζ_{θ_x}, ζ_{θ_y}	=	damping ratio of the support in roll and pitch modes
θ_x, θ_y	=	body modes in roll and pitch
ξ_1, ξ_2	=	nondimensional blade segments
ξ_h	=	nondimensional rotor height, $\bar{h}/I$
σ_j	=	modal damping (real part of s_j)
τ	=	nondimensional time, Ωt
$\bar{\phi}_i$	=	rotating mode shape
ϕ_x	=	comparison functions
ψ_i	=	elastomer deformation in ith lag mode
Ω	=	angular velocity of the rotor
ω	=	excitation frequency
$\hat{\omega}_i$	=	ith frequency of rotating blade
ω_{Ni}	=	nonlinear frequency
ω_x, ω_y	=	support structure frequencies

Received 12 October 2001; revision received 22 March 2004; accepted for publication 20 November 2003.

*Graduate Student, Department of Mechanical Engineering; currently Reader, Department of Mechanical Engineering, Jadavpur University, Calcutta, India.

†Professor, Department of Aerospace Engineering. Senior Member AIAA.

‡Professor, Department of Mechanical Engineering.

Introduction

WITH the advancement in technology, development of a mechanically simple yet efficient rotor blade system has resulted in the design of bearingless blade and hub configuration. A schematic diagram of a bearingless rotor blade is shown in Fig. 1. In this rotor system, the blade is attached to the hub through a flexbeam, which is designed to provide the required stiffness in the flap and lag bending deformation of the blade, but it is highly flexible in torsion. Surrounding the flexbeam, there is a stiff cuff denoted as torque tube, which is attached to the blade-flexbeam junction at the outboard end and to a pitch link at the inboard end as shown in Fig. 1. The pitch control of the blade is achieved by rotating the torque tube through up/down movement of the point P, which in turn twists the flexbeam. An elastomer is placed between the torque tube and flexbeam to provide adequate lag damping. It also serves the purpose of a spacer between the torque tube and the flexbeam. Though a bearingless rotor is mechanically simple, its dynamic analysis becomes complicated due to the presence of multiple load path and nonlinear elastomeric damper.

When the helicopter is on ground, the dynamic coupling between rotor and body degrees of freedom leads to instability, commonly denoted as ground resonance. The rotor lead-lag regressive mode usually couples with the body pitch and/or body roll to cause this

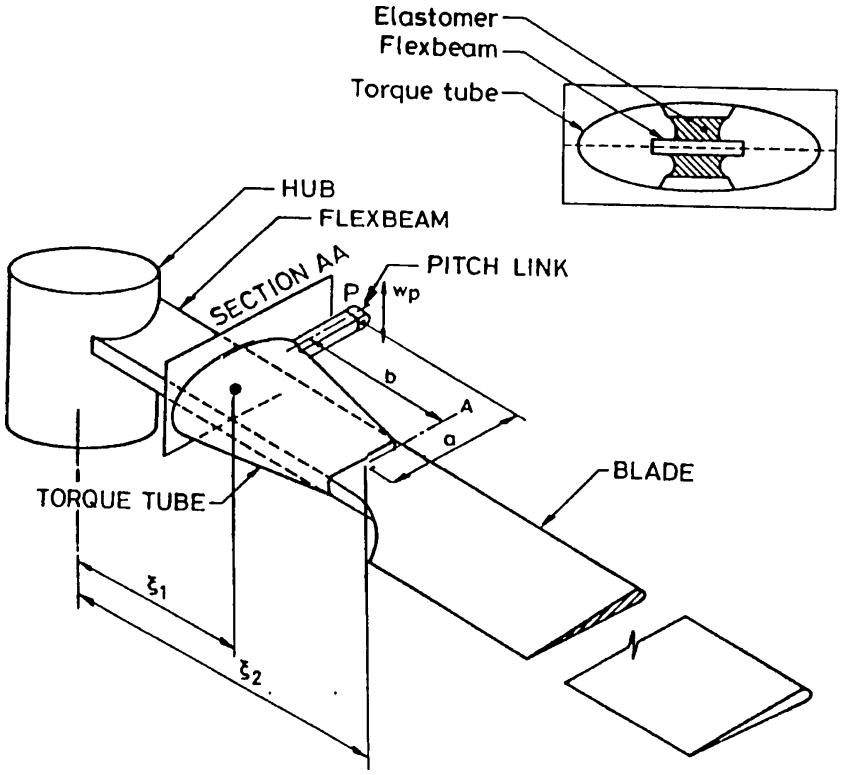

Fig. 1 Bearingless rotor blade with pitch link at the leading edge.

instability. In the case of bearingless rotor system, the ground resonance is avoided by providing elastomeric damper to the rotor blade and damping in the landing gear.

One of the earliest analytical models for bearingless rotors was developed by Hodges.[1,2] Chopra and his associates[3–7] reported several studies using the finite element method to determine the periodic response and stability of a bearingless rotor blade. Gandhi and Chopra[6] analyzed the ground/air resonance stability of a helicopter model with nonlinear elastomeric lag damper. In their study, the blade is assumed to be rigid with a root hinge simulating both the articulated and hingeless rotor systems. A nonlinear elastomer, placed at the lag hinge and consequently having the same displacement as that of the blade in lag mode, was considered. Performing a linearized stability analysis, they observed that the nonlinear elastomeric damper has a stabilizing influence on ground/air resonance.

Recently, Panda and Mychalowycz[8] presented a correlation of wind-tunnel tests and analytical studies for a scaled model of a Comanche bearingless main rotor. The model was tested with both fluidlastic (linear characteristics) and elastomeric (nonlinear characteristics) dampers. The experimental results indicated that the nonlinearities in stiffness and loss factor seem to have a significant influence on the limit-cycle oscillations. The fluidlastic damper because of its linear nature does not exhibit any limit-cycle oscillation. In their analytical model, the elastomer was treated as a linear element. Ormiston et al.[9] investigated the aeromechanical stability of hingeless and bearingless rotors. They considered an elastomer model in which the damping force was assumed to be proportional to a linear combination of different powers of velocity (powers of $\frac{1}{2}$, 1, 2, and 3). Using this nonlinear elastomer model, they showed the phenomenon of limit-cycle oscillations of the system. They concluded that the effects of nonlinear dampers are significant and complex. Until the ideal bearingless rotor without auxiliary lead-lag dampers is developed, the modeling and behavior of elastomeric dampers warrant additional attention.

Analysis of bearingless rotor blade requires a blade model including the nonlinearities of the elastomer stiffness and damping. In the following, a brief description of the static and dynamic behavior of the elastomer is provided to bring out the essential difference between linearized stiffness and amplitude-dependent stiffness and

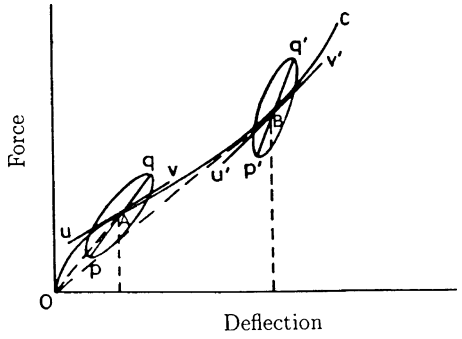

Fig. 2 Nonlinear dynamic characteristics of a viscoelastic material.

damping. Because of the viscoelastic nature of the material, damping and stiffness properties of the elastomer are complex functions of the displacement amplitude, frequency and temperature. A typical static load deflection curve for a nonlinear viscoelastic material is shown in Fig. 2 by the curve *OABC*. Generally the static nonlinear characteristics of the elastomer are described by the secant stiffness evaluated at different values of deflection. For example, the secant stiffnesses at points *A* and *B* are defined by the slopes of the line *OA* and *OB* (Fig. 2), respectively.

The load-deflection curve of the elastomer under a sinusoidal displacement input about these two equilibrium points *A* and *B* can be represented by the corresponding viscoelastic hysteresis loops superimposed on the equilibrium curve *OABC* at the points *A* and *B*, respectively. The dynamic stiffness values at *A* and *B* are defined by the slopes of the line pq and $p'\,q'$, where the points p, q', p', and q' are the points corresponding to the maximum deflection of the elastomer as shown in Fig. 2. On the other hand, linearized stiffness is defined using static load-deflection curve. The slopes of the tangent lines uv and $u'v'$ represent the linearized stiffness values in the vicinity of the equilibrium points *A* and *B*, respectively. The details of these definitions can be found in Refs. 10 and 11.

In most cases, the dynamic tests on an elastomer are carried out without any static preloading, that is, about an equilibrium position

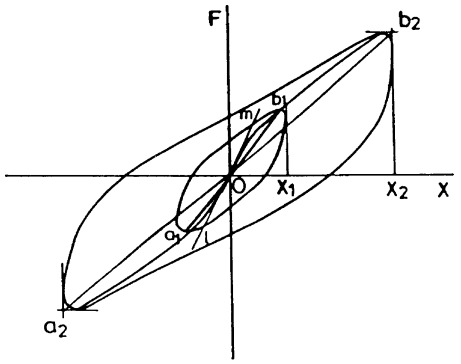

Fig. 3 Hysteresis cycles of a nonlinear material about zero equilibrium point.

with zero deformation. The material is subjected to a harmonic displacement excitation, and the required force is measured. Using the input-output time response, the stiffness and damping modulii of the elastomer are identified. A clear description of the definition of these quantities and the mathematical approach for identification of these quantities from test data are given in Ref. 12. The stiffness modulus is defined as the in-phase force component that is required to produce unit amplitude of deformation. Similarly, the damping modulus is defined as the required force component (for unit amplitude of deformation) that is in quadrature to the deformation. The dynamic stiffness and damping values can also be identified from hysteresis cycles for different amplitudes of motion. The area of the hysteresis loop provides the information about the amount of energy dissipated per cycle at a particular amplitude of deformation. Typical hysteresis cycles of a nonlinear elastomeric material about zero equilibrium position are shown in Fig. 3. It can be observed from Fig. 3 that when the amplitude of motion is X_1 the corresponding dynamic stiffness is given by the slope of the line a_1b_l. When amplitude of motion is increased to X_2, the slope of the line a_2b_2 represents the dynamic stiffness. It is evident that these two stiffness values can be different depending on the distortion of the hysteresis loop with the amplitude of motion. However, the linearized stiffness about the zero equilibrium point is given by the slope of the static load deflection curve $a_2a_1Ob_1b_2$ at O, that is, slope of the line lm. The value of linearized stiffness can be different from the dynamic stiffness for a given amplitude. Also, the dynamic stiffness is a function of the amplitude of motion. The energy dissipated by the viscoelastic material for a particular amplitude of motion is given by the area of the corresponding hysteresis loop. Figure 3 also indicates that the energy dissipation per cycle depends on the amplitude of motion. In case of a linearized analysis, a damping value has to be chosen based on an arbitrary value of amplitude of motion.

The preceding discussion clearly indicates that the elastomer model should capture the non-linear behavior of the material so far as the stiffness and damping are concerned. In addition, it should be possible to integrate the model easily with a structural dynamic model of a rotor blade for subsequent aeroelastic and aeromechanical analysis without neglecting the effect of the amplitude of motion on the elastomer characteristics.

The nonlinear dynamic characteristics of the elastomer are usually represented by the variation of in-phase stiffness (stiffness) and quadrature stiffness (damping) as a function of amplitude. The experimental results of a single-frequency bench test can be found in Refs. 12–15. The data given in Ref. 15 are reproduced in Fig. 4. The figure indicates that both the in-phase stiffness (denoted as K') and the quadrature stiffness (denoted as K'') decrease as the amplitude of motion increases. The variation of loss tangent or loss factor η with amplitude is also shown in the figure. Loss tangent is generally defined as the ratio of K'' and K'. It can be noticed that there is no decrease in the quadrature stiffness at very low amplitude of motion for all of the experimental data. However, as shown in Fig. 4c, the computed loss factor η decreases at low amplitudes. The reason for the decrease in loss factor at low amplitude of motion is mostly a

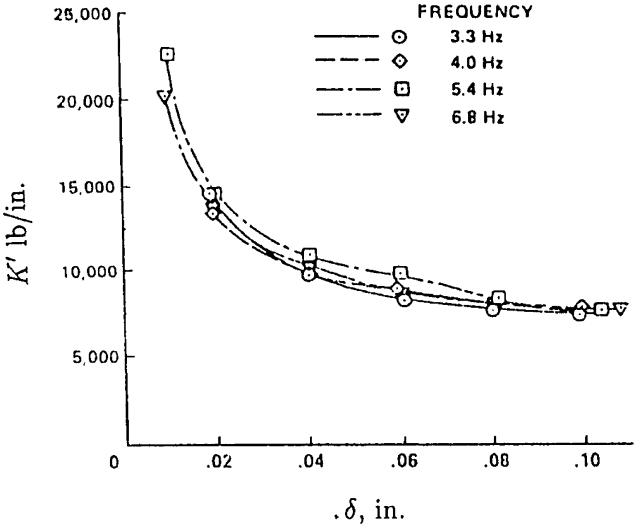

a) In-phase stiffness

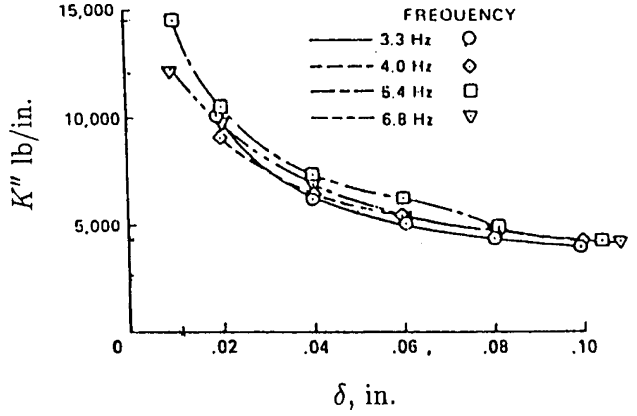

b) Quadrature stiffness

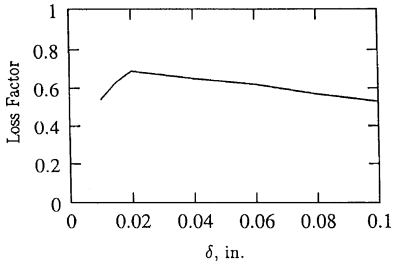

c) Loss factor (computed)

Fig. 4 Experimenta data taken from Ref. 15.

result of the sharp rise in the value of in-phase stiffness K' at low amplitude. In a recent publication, Kunz[16] also indicated a similar type of stiffness and damping characteristics of the elastomer with respect to amplitude of motion. He pointed out that nonlinear Voigt–Kelvin–solid model was suitable for prediction of forced response. However, this elastomer model was found to be amplitude dependent. Therefore, special attention must be paid while using this model in dynamic analysis.

There are several linear models to describe the mechanical behavior of viscoelastic materials, for example, anelastic displacement fields (ADF) have been used in Ref. 17. Smith et. al.[18] extended the method of ADF to include the nonlinearities and temperature effects.[19] The nonlinear characteristics of elastomer have been analyzed in detail in several recent publications.[20–26] In Ref. 12, the authors have proposed a stiffness-viscosity-elasto-slide model, having a Kelvin chain and an elasto-slide element in parallel, to capture the time-domain and frequency-domain characteristics of the elastomer. A model, comprising a quartic spring and a linear Kelvin

element, which is suitable for integration with a blade model for subsequent aeroelastic studies, has been proposed by Gandhi and Chopra.[7] In this model, the values of the parameters were determined by fitting the analytical curves with the experimental data. Another approach based on fractional derivatives has also been developed to model the nonlinear characteristics of the elastomer.[26]

The review of the literature clearly indicates that the elastomer used in a bearingless rotor shows highly nonlinear characteristics both in stiffness and damping with respect to amplitude of deformation. Therefore, it is expected that because of the presence of the elastomer the lag and flap frequencies should be dependent on the amplitude of motion, which is a typical feature that distinguishes a nonlinear system from a linear one.

Several researchers have proposed different nonlinear models with a varying degree of complexity to capture the nonlinear characteristics of the elastomer. However, while performing the stability analysis by eigensolution approach, only the linearized equations of the blade and elastomer about the equilibrium points are solved. Hence, the dependence of stiffness and damping characteristics of the elastomer on the amplitude of motion is treated through equivalent linearization approach. However, if the influence of magnitude of initial disturbance on the stability of the system is to be studied then one might have to resort to time-domain response analysis of the nonlinear equations of motion.

In this paper, a comparison of the results of linearized stability analysis and the time-domain response of fully nonlinear equations is made to bring out the effect of nonlinearity on the stability of a dynamic system. The example problem chosen for this comparison is the dynamic stability of an idealized bearingless rotor (with a nonlinear elastomer) and fuselage system under ground resonance condition.

The objectives of the present study are to 1) formulate a simple nonlinear model for the elastomer, which is amenable to subsequent integration with the blade model for ground resonance analysis; 2) study the influence of amplitude of motion of the isolated lag dynamics of the blade; 3) analyze the effects of amplitude dependence of elastomer characteristics on the stability of rotor-fuselage system under ground resonance condition (This study is carried out by equivalent linearization of elastomer properties followed by eigenanalysis.); 4) analyze the ground resonance stability by directly integrating the governing nonlinear differential equations in time domain, for different operating and initial conditions; and 5) provide a comparative study of the results of ground resonance obtained by the two approaches (namely, eigenapproach and time integration) to understand the influence of nonlinearities of the elastomer.

Elastomeric Damper Model

The nonlinear characteristics of the elastomeric material can be idealized by a combination of linear and nonlinear restoring and dissipative elements. Because the static stress–strain curve of an elastomeric material is nonlinear, it is logical to assume the restoring element to be nonlinear. The experimental results[12–15] of an elastomeric lag damper under single frequency excitation show that both in-phase K' and quadrature K'' stiffness decrease as the amplitude of motion increases, but neither of them display any significant dependence on frequency within the range of interest (3.3–6.4 Hz) as shown in Fig. 4. (It can be noted that the elastomer exhibits a highly complex behavior under multiple frequency excitation inputs.[12,15]) Figure 5 represents an idealized model consisting of a nonlinear spring, a Coulomb damper, and a hysteretic damper. The reason for choosing a Coulomb damper is that the damping force is very high at low amplitude. In addition, Coulomb and hysteretic dampers provide damping forces that are independent of frequency. This type of idealization differs from the model proposed by Gandhi and chopra, in the sense that their model has a viscous damping element. The constitutive differential equation of the elastomer model under harmonic loading can be written as, respectively,

$$K_1 x - K_3 x^3 + K_5 X^5 - K_7 X^7 + F \operatorname{sgn} |\dot{x}| + (h_1/\omega)\dot{x} = D_\circ \sin \omega t \tag{1}$$

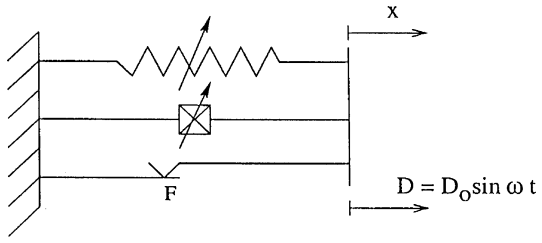

Fig. 5 Elastomer model.

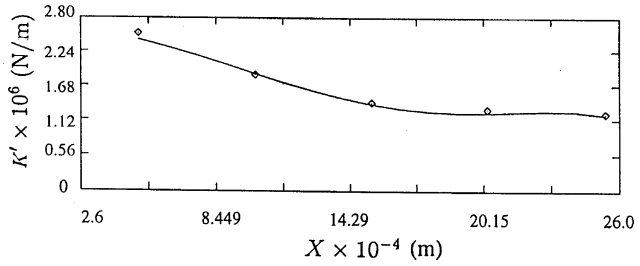

Fig. 6 Variation of K' (in-phase stiffness) with amplitude: ◇, experimental data; ——, proposed model.

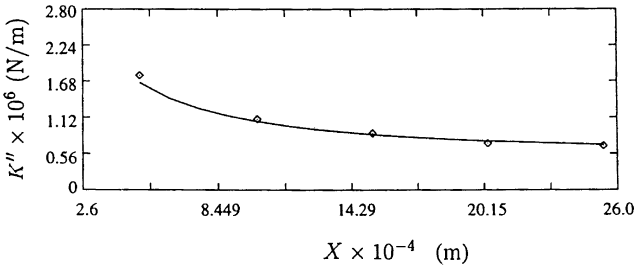

Fig. 7 Variation of K'' (quadrature stiffness) with amplitude: ◇, experimental data; ——, proposed model.

Assuming a harmonic motion and following the procedure mentioned in Refs. 27 and 28, the in-phase stiffness K' and the quadrature stiffness K'' of the elastomer can be obtained as

$$K' = K_1 - \tfrac{3}{4}K_3X^2 + \tfrac{5}{8}K_5X^4 - \tfrac{1}{2}K_7X^6 \tag{2}$$

and

$$K'' = 4F/\pi X + h_1 \tag{3}$$

where X is the amplitude of motion. The stiffness and damping parameters have been obtained by correlating the theoretical and experimental data points and using least-square error minimization approach, described in Ref. 27. The values of the parameters are identified to be $K_1 = 2.6739 \times 10^6$ N/m, $K_3 = 1.3152 \times 10^{12}$ N/m^3, $K_5 = 3.5195 \times 10^{17}$ N/m^5, $K_7 = 3.17625 \times 10^{22}$ N/m^7, $F = 4.7973 \times 10^2$ N, and $h_1 = 4.5691 \times 10^5$ N/m. Figures 6 and 7 show the comparison of the experimental data with the theoretical results obtained using the idealized elastomer model. It is evident from Figs. 6 and 7 that the proposed model correlates well with the experimental data. For the sake of information, the hysteresis loops of the elastomer model for two different amplitudes of motion are shown in Fig. 8.

Nonlinear Dynamics of Lag Motion

Before proceeding to analyze the effect of nonlinear elastomer on ground resonance problem, it is instructive to study the nature of amplitude-dependent frequency of lag mode as a result of elastomer nonlinearity. In this section, the influence of elastomer nonlinearity on the undamped lag natural frequencies of a rotating blade has been studied. An idealized model of a bearingless rotor is shown in Fig. 9. The torque tube is represented by a massless rigid link EC. The

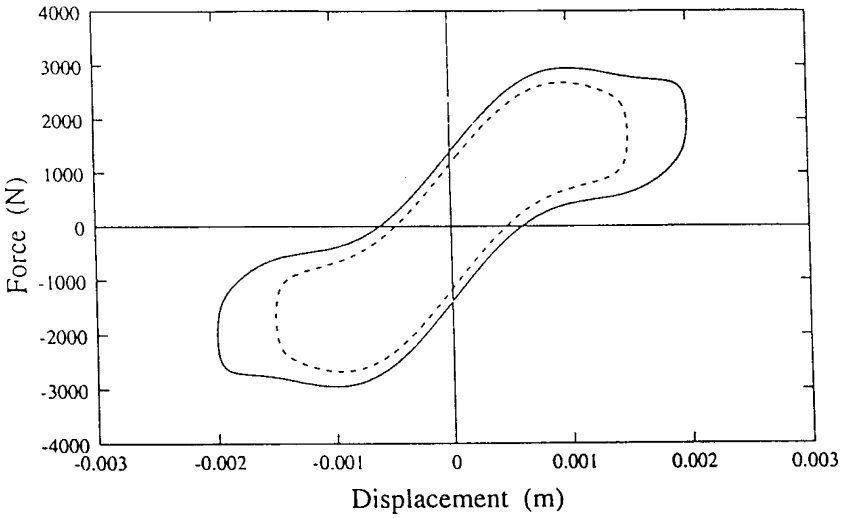

Fig. 8 Comparison of the hysteresis curves for different amplitude of motions: ——, $X = 0.002$ m; – – – –, $X = 0.0015$ m.

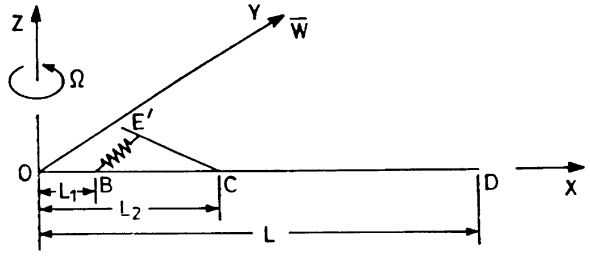

Fig. 9 Idealized bearingless rotor blade.

blade is assumed to be an Euler–Bernoulli beam undergoing only lag deformation. Because damping does not play any significant role so far as the natural frequencies are concerned, elastomer is represented by only a spring element. Thus, the bearingless rotor can be idealized as a rotating beam having a nonlinear spring connected between the points B and C on the beam through the torque tube.

The elastomer is represented by the seventh-order nonlinear spring. Following Pakdemirli and Nayfeh,[29] a numerical-perturbation technique is adopted to evaluate the amplitude-dependent-frequency relations for various elastic modes in lead lag.

The kinetic energy of the beam under isolated lag motion is given by

$$T(t) = \frac{1}{2}\int_{\theta}^{L} m\left[\left(\frac{\partial \bar{u}}{\partial t} - \Omega\bar{v}\right)^2 + \left(\frac{\partial \bar{v}}{\partial t} + \Omega x + \Omega\bar{u}\right)^2\right] \mathrm{d}x \quad (4)$$

Assuming that the blade is very stiff in the axial direction, the following inextensibility condition is imposed:

$$\bar{u} = -\frac{1}{2}\int_{0}^{x}\left(\frac{\partial \bar{v}}{\partial x^2}\right)^2 \mathrm{d}x \quad (5)$$

The expression for strain energy caused by in-plane bending is

$$U_1 = \frac{1}{2}\int_{0}^{L} EI\left[\frac{\partial^2 \bar{v}(x,t)}{\partial x^2}\right]^2 \mathrm{d}x \quad (6)$$

The strain energy of the spring as a result of deformation Δ_l in the lag direction is given by

$$U_2 = \tfrac{1}{2}K_1\Delta_l^2 - \tfrac{1}{4}K_3\Delta_l^4 + \tfrac{1}{6}K_5\Delta_l^6 - \tfrac{1}{8}K_7\Delta_l^8 \quad (7)$$

where

$$\Delta_l = \left[\bar{v}(L_2,t) - (L_2 - L_1)\frac{\partial \bar{v}(L_2,t)}{\partial x} - \bar{v}(L_1,t)\right] \quad (8)$$

Assuming a solution in the form

$$v(\xi, r) = \sum_{i=1}^{n} \hat{\phi}_i(\xi) q_i(\tau) \quad (9)$$

and using the Rayleigh–Ritz approach, the temporal equation of motion in lag mode can be obtained as

$$[M]\{\ddot{q}\} + [K]\{q\} + \{F_{\mathrm{NL}}\{q\}\} = 0 \quad (10)$$

where $F_{\mathrm{NL}}\{q\}$ contains the contribution of the nonlinear terms in the spring force.

To decouple the linear part of the preceding equation, the following linear transformation is introduced:

$$q(\tau) = [P]z(\tau) \quad (11)$$

where $[P]$ is formed by the normalized eignvector of the linear eigenvalue problem obtained after neglecting the nonlinear terms in Eq. (10).

Substituting Eq. (11) in Eq. (10) and premultiplying by $[P]^T$, the temporal equation is obtained in the form

$$\ddot{z}_i(\tau) + \hat{\omega}_i^2 z_i(\tau) - \varepsilon\alpha_3 \sum_{m=1}^{n}\sum_{s=1}^{n}\sum_{r=1}^{n} \Gamma_{\mathrm{imsr}} z_m z_s z_r + \varepsilon^2\alpha_5 \sum_{m=1}^{n}\sum_{s=1}^{n}\sum_{r=1}^{n}\sum_{t=1}^{n}\sum_{u=1}^{n} \Gamma_{\mathrm{msrtu}} z_m z_s z_r z_t z_u - \varepsilon^3\alpha_7 \sum_{m=1}^{n}\sum_{s=1}^{n}\sum_{r=1}^{n}\sum_{t=1}^{n}\sum_{u=1}^{n}\sum_{v=1}^{n}\sum_{w=1}^{n} \Gamma_{\mathrm{msrtuvw}} \times z_m z_s z_r z_t z_u z_v z_w = 0 \qquad i = 1, 2, 3, \ldots, n \quad (12)$$

where $\hat{\omega}_i$ is ith linear natural frequency, ε is a small nondimensional parameter, and

$$\Gamma_{\mathrm{lmsr}} = \bar{\Psi}_i\bar{\Psi}_m\bar{\Psi}_s\bar{\Psi}_r, \quad \Gamma_{\mathrm{lmsrtu}} = \bar{\Psi}_i\bar{\Psi}_m\bar{\Psi}_s\bar{\Psi}_r\bar{\Psi}_t\bar{\Psi}_u$$

$$\Gamma_{\mathrm{lmsrtuvw}} = \bar{\Psi}_i\bar{\Psi}_m\bar{\Psi}_s\bar{\Psi}_r\bar{\Psi}_t\bar{\Psi}_u\bar{\Psi}_v\bar{\Psi}_w$$

$$\alpha_3 = K_3L/m\Omega^2, \qquad \alpha_5 = K_5L^3/m\Omega^2, \qquad \alpha_7 = K_7L^5/m\Omega^2$$

and

$$\bar{\Psi}_i = \hat{\Psi}_1 p_{1i} + \hat{\Psi}_2 p_{2i} + \cdots + \hat{\Psi}_n p_{\mathrm{ni}} \quad (13)$$

where

$$\hat{\Psi}_i = \hat{\phi}_i(\xi_2) - (\xi_2 - \xi_1)\hat{\phi}_i'(\xi_2) - \hat{\phi}_i(\xi_1) \tag{14}$$

$\hat{\Psi}_i$ can be interpreted as the deformation of the spring in ith lag mode. In Eq. (13), p_{ij} represent the elements of the matrix $[P]$.

Then, following the method of multiple timescales the nonlinear frequency ω_{Ni} and amplitude $\hat{A}_i$ relation for the ith mode can be obtained as

$$\omega_{\mathrm{Ni}} = \hat{\omega}_i - \frac{3}{8\omega_i}\alpha_3\Gamma_{4i}\hat{A}_i^2 - \frac{15}{256\omega_i^3}\alpha_3^2\Gamma_{4i}^2\hat{A}_i^4 + \frac{5}{16\omega_i}\alpha_5\Gamma_{6i}\hat{A}_i^4 + \frac{5}{64\omega_i^3}\alpha_3\Gamma_{4i}\alpha_5\Gamma_{6i}\hat{A}_i^6 - \frac{111}{64\times 128\omega_i^5}\alpha_3^3\Gamma_{4i}^3\hat{A}_i^6 - \frac{35}{128\omega_i}\alpha_7\Gamma_{8i}\hat{A}_i^6 \tag{15}$$

where $\hat{\omega}_i$ is ith linear natural frequency; α_3, α_5, α_7 are nondimensional stiffness parameters [as defined in Eq. (13)]; and $\Gamma_{4i} = (\bar{\Psi}_i)^4$, $\Gamma_{6i} = (\bar{\Psi}_i)^6$, $\Gamma_{8i} = (\bar{\Psi}_i)^8$.

Ground Resonance Analysis

An idealized model of the coupled rotor/fuselage system is shown in Fig. 10. The blade is assumed to undergo only lag motion. The elastomer is represented by nonlinear spring and damping elements. The torque tube is assumed to be rigid and massless. The effect of pitch link in the lag mode is neglected. The hub is located at a height h above the c.g. of the fuselage. The fuselage is allowed to undergo rigid body pitch θ_y and roll θ_x motions. The characteristics of the fuselage support (landing gear) is represented by a linear spring and a linear damper. Because emphasis is placed on the effect of nonlinearity of the elastomer on the ground resonance problem, the aerodynamic effects are not considered.

Stability by Eigenanalysis (Linearised Equation)

The dynamical equations of motion of the coupled rotor/fuselage model consist of two sets of equations: one corresponding to the blade motion and the other representing the motion of the fuselage. Because pitch and roll motions of the fuselage introduce additional inertia effects, they must be included in the equation of lag motion of the blade. The strain energy of the nonlinear spring caused by the deformation Δ_i is

$$U_2 = \tfrac{1}{2}K_{\mathrm{eq}}(\Delta_l)\Delta_l^2 \tag{16}$$

where K_{eq} is the equivalent stiffness, which is dependent on the amplitude of motion of the blade.

The work done by the dissipative element of the elastomer is given by

$$W_d = \tfrac{1}{2}C_{\mathrm{eq}}(\Delta_l)\dot{\Delta}_l^2 \tag{17}$$

where C_{eq} is the equivalent (amplitude-dependent) damping coefficient. The equivalent stiffness K_{eq} and damping C_{eq} are obtained from the dynamic stiffness K' and damping K'' for a given amplitude of the elastomer. Accordingly, one can write

$$K_{\mathrm{eq}} = K_1 - \tfrac{3}{4}K_3X^2 + \tfrac{5}{8}K_5X^4 - \tfrac{1}{2}K_7X^6$$

$$C_{\mathrm{eq}} = k_1/\omega + 4F/\pi\omega X$$

where X is the amplitude of motion of the elastomer.

The nondimensional lag deformation of the kth blade is assumed to be of the form:

$$v_k(\xi,\tau) = \sum_{i=1}^{n1}\bar{\phi}_i(\xi)z_{ik}(\tau) \tag{18}$$

where $\bar{\phi}_i$ is the ith rotating mode shape of the kth blade and $n1$ is the number of rotating modes. Because the equivalent stiffness of the elastomer is a function of the amplitude of motion, the rotating mode shapes and frequencies will also be functions of amplitude of motion.

Considering only the first lag mode of each blade and applying multi-blade-coordinate transformation, blade equations are converted into equations in rotor degrees of freedom. The collective and alternating modes are neglected as these do not participate in the ground resonance problem.

The cyclic lag equations for the elastic lag mode can be written as

$$\ddot{z}_{1c} + \bar{C}\dot{z}_{1c} + 2\dot{z}_{1s} + \left(\omega_1^2 - 1\right)z_{1c} + \bar{C}z_{1s} - p\ddot{\theta}_x = 0$$

$$\ddot{z}_{1s} + \bar{C}\dot{z}_{1s} - 2\dot{z}_{1c} + \left(\omega_1^2 - 1\right)z_{1s} - \bar{C}z_{1c} - p\ddot{\theta}_y = 0$$

where $p = \xi_k\int_0^1\bar{\phi}_i\,\mathrm{d}\xi$ and $\bar{C} = C^*(\hat{\Psi}_1)^2$.

The forces acting on the hub can be obtained by resolving the blade-root shear forces in the nonrotating frame and summing over all the N blades. Considering the support structure as a combination of mass-spring-damper system having pitch and roll motions,

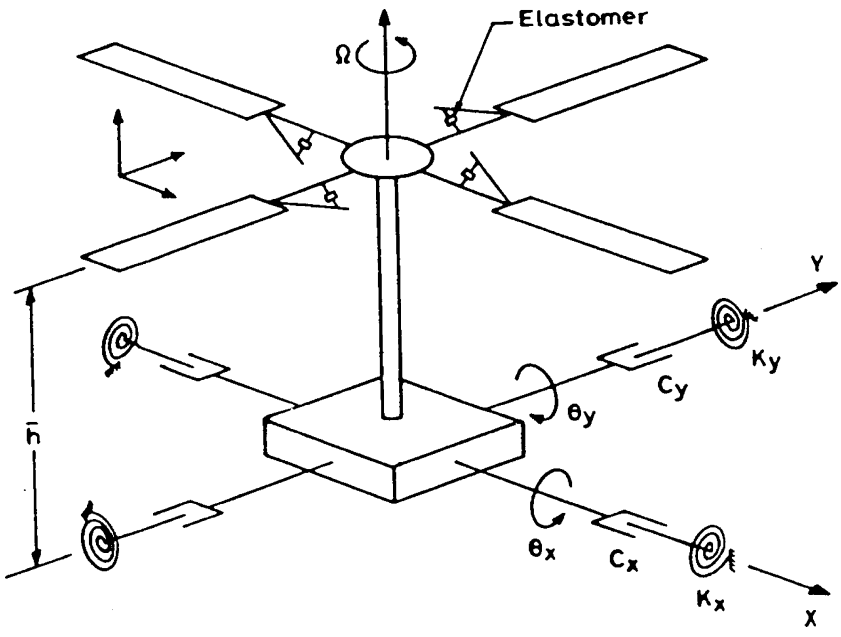

Fig. 10 Idealized model of the coupled rotor/fuselage system.

the equations of motion of the support in nondimensional form are written as

$$I_y\ddot{\theta}_y + C_y\dot{\theta}_y + K_y\theta_y - (N/2)p\ddot{z}_{1s} = 0$$

and

$$I_x\ddot{\theta}_x + C_x\dot{\theta}_x + K_x\theta_x - (N/2)p\ddot{z}_{1c} = 0$$

The preceding four equations are arranged in the form

$$[\bar{M}]\{\ddot{X}\} + [\bar{C}]\{\dot{X}\} + [\bar{K}]\{X\} = 0 \tag{19}$$

where $\bar{M}$, $\bar{C}$, and $\bar{K}$ are the mass, damping, and stiffness matrices, respectively. The vector $\{\boldsymbol{X}\}$ represents the degrees of freedom, that is,

$$\{\boldsymbol{X}\} = \{z_{1c}\, z_{1s}\, \theta_y\, \theta_x\}^T \tag{20}$$

The ground resonance stability is determined by the eigenvalues of the 8×8 matrix $[\boldsymbol{G}]$, where

$$[\boldsymbol{G}] = \begin{bmatrix} 0 & I \\ \bar{M}^{-1}\bar{K} & -\bar{M}^{-1}\bar{C} \end{bmatrix} \tag{21}$$

Response Analysis in Time Domain (Nonlinear Equation)

The coupled rotor/fuselage nonlinear equations of motion in time domain are obtained by writing the equations of equilibrium for each blade in lag mode (one mode per blade) and pitch and roll equations of the fuselage about its center of mass. The equations can be written in symbolic form as

$$[\hat{M}]\{\ddot{Y}\} + [\hat{C}]\{\dot{Y}\} + [\hat{K}]\{Y\} + [\hat{F}_{\mathrm{NL}}(Y, \dot{Y}, \ddot{Y})] = 0 \tag{22}$$

Assuming a four-bladed rotor system, the vector $\{\boldsymbol{Y}\}$ represents the degrees of freedom, that is,

$$\{\boldsymbol{Y}\} = \{z_{11}\, z_{12}\, z_{13}\, z_{14}\, \theta_y\, \theta_z\}^T \tag{23}$$

The vector $\{\hat{F}_{\mathrm{NL}}(Y, \dot{Y}, \ddot{Y})\}$ includes all of the nonlinear terms. The mass matrix $\lfloor\hat{M}\rfloor$ and damping matrix $\lfloor\hat{C}\rfloor$ are periodic because of participation of fuselage degrees of freedom in blade equations and the dependence of fuselage motion on the azimuthal location of the blade. The reason for the periodic nature of these matrices is that the blade equations are written in rotating frame and the fuselage equations are given in nonrotating frame.

Solution Procedure

The method of solution depends on the type of analysis. In the following, the solution procedure adopted for eigen analysis and time domain analysis are presented.

Stability by Eigenanalysis

The step-by-step technique for analyzing the amplitude-dependent stability of the coupled rotor-fuselage system is described next:

1) For a prescribed amplitude of motion of the elastomer, equivalent stiffness K_{eq} and damping C_{eq} are evaluated.

2) Using K_{eq}, the natural frequency ω_i and the corresponding mode shape $\bar{\phi}_i$ of the rotating blade in the lag mode are determined.

3) Because only the first lag mode is considered in the ground resonance problem, using the mode shape $\bar{\phi}_i$ the quantities $\bar{C}$ and p are evaluated.

4) Knowing $\bar{M}$, $\bar{C}$, and $\bar{K}$ [Eq. (19)] an eigenanalysis of matrix $\boldsymbol{G}$ is performed to determine the stability of the system under ground resonance condition. The eigenvalues appear as complex conjugate pairs $s_j = \sigma_j \pm i\omega_j$, where ω_j represents the frequency of the mode and σ_j represents the modal damping. The mode is stable if σ_j is negative and unstable when σ_j is positive.

Because the lag mode shape is dependent on the operating conditions, and the blade and elastomer parameters, for any change in these parameters the preceding steps have to be repeated.

Stability by Response Analysis

In this method, the stability of the system is qualitatively determined by inspecting the time response of the system to a given magnitude of initial condition. The time response of the coupled rotor/fuselage system is obtained by simultaneously solving the nonlinear coupled equations by numerical integration technique in time domain at every time step. The mass matrix as $[\hat{M}]$ and $\lfloor\hat{C}\rfloor$ in Eq. (22) are time dependent. Therefore, the mass matrix $[\hat{M}]$ has to be inverted at every time step. Based on the convergence/divergence of the response, the stability of the system can be established.

Results and Discussion

The numerical results are presented in three sections. In the first section, the results pertaining to frequency-amplitude relationship of the uncoupled lag motion are discussed. In the next section, the results pertaining to ground resonance problem by eigenanalysis are presented. In the third section, the results of the response analysis are described. The data used for the analysis are given in Table 1.

Frequency-Amplitude Relationship

The frequency-amplitude relation for the ith mode is obtained from Eq. (15). Variation of the first natural frequency with the amplitude of oscillation at the free end of the blade is shown in Fig. 11. The first natural frequency decreases monotonically with increasing amplitude. A similar behaviour is also observed for the second natural frequency.[26]

Figure 12 shows the nature of variation of the nonlinear first natural frequency with amplitude as one uses different orders of approximation for the spring. With the inclusion of higher-order nonlinear term (one at a time), the frequency-amplitude relationship shows alternate softening and stiffening nature. This is because of the alternating signs in the polynomial, expressing the restoring force. Consequently, one can conclude that the nonlinear natural frequency is somewhat insensitive to the value of amplitude of oscillation.

Table 1 Input data

Parameters	Value
Blade data	
Mass per unit length, m	9.7 kg/m
Length	6.6 m
$\bar{\alpha}(= EL/m\Omega^2L^4)$	0.0301
Rotor angular velocity, Ω	32.8 rad/s
Numbers of blades	4
Nondimensional fuselage data	
Mass moment of inertia (roll), I_x	1.0511
Mass moment of inertia (pitch), I_y	3.1023
$\xi_h = \bar{h}/L$	0.2
$\omega_x = (K_x/I_x)^{1/2}$(roll)	$(4/\Omega) \times 2\pi$
$\omega_y = (K_y/I_y)^{1/2}$(pitch)	$(2/\Omega) \times 2\pi$
$C_x = 2\zeta_{\theta_x}\omega_x$, $C_y = 2\zeta_{\theta_y}\omega_y$	

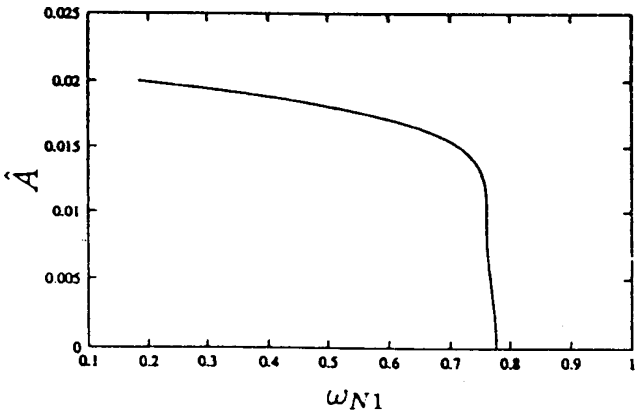

Fig. 11 Variation of first nonlinear frequency with amplitude of oscillation in lag mode.

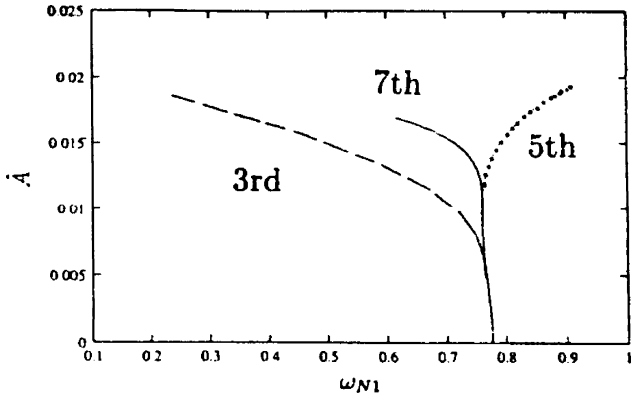

Fig. 12 Influence of different orders of approximation on the first natural frequency in lag mode.

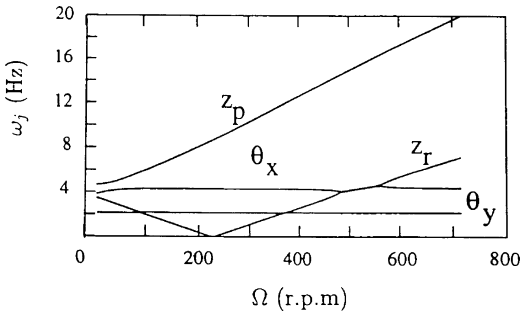

Fig. 13 Variation of modal frequencies as a function of rotational speed: $\xi_1 = 0.1$, and $\xi_2 = 0.25$.

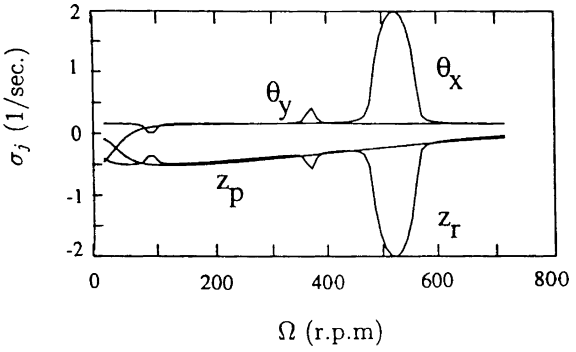

Fig. 14 Variation of modal damping as a function of rotational speed: $\xi_1 = 0.1$, and $\xi_2 = 0.25$.

Stability by Eigenanalysis

A thorough investigation is carried out to study the influence of the elastomer on the ground resonance stability of a bearingless rotor. The number of blades in the rotor system is assumed to be four. The elastomer is idealized as a combination of a nonlinear spring, a Coulomb damper, and a hysteretic damper. For the baseline configuration, the locations of the elastomer and torque tube are set at $\xi_1 = 0.1$ and $\xi_2 = 0.25$ (Fig. 1). The length data are nondimensionalized with respect to blade length. The damping in pitch and roll modes of the fuselage is assumed to be zero ($C_x = C_y = 0$). The amplitude of motion of the elastomer is taken as 0.00015 (0.001 m). Following the steps mentioned in the section on stability by eigenanalysis, the eigenvalues of the matrix $\boldsymbol{G}$ are calculated. Figures 13 and 14 show the variation of the modal frequencies ω_j and damping σ_j, respectively, as a function of rotational speed Ω. Figure 13 indicates that the coalescence of the regressive lag mode Z_r with fuselage modes in pitch θ_y and roll θ_x occurs at three regions of rotational speed (namely, 85–100 rpm, 350–400 rpm, and 440–600 rpm). In the range 350–400 rpm, θ_y is unstable having maximum instability with $\sigma_j = 0.23\ \mathrm{s}^{-1}$ whereas in the rpm range 440–600, θ_x is unstable with a maximum positive value of $\sigma_j = 1.67\ \mathrm{s}^{-1}$. The coalescence of Z_r with θ_y occurring at a very low rpm range 85–95 does not produce any instabilities in the system. The progressive mode Z_p is always stable with a slight variation in damping levels.

While describing additional stability results in the following, the frequency diagram is not presented because the nature of frequency variation of different modes and their coalescence are observed to be similar for all cases.

Effect of Amplitude

Numerical results are obtained for three different values of the nondimensionalized amplitude of motion of the elastomer in lag mode corresponding to 0.000075, 0.00015 and 0.0003. Figure 15 shows the variation of modal damping as a function of rotor rpm for all of the modes. The results indicate that for this configuration the amplitude of elastomer motion has very little effect on damping in all modes with the exception of progressive lag mode. It is observed that the damping in progressive lag mode decreases with increase in amplitude of elastomer motion. In addition, the rpm range of instability is not affected by the variation in the amplitude of elastomer motion.

Influence of Elastomer Location (ξ_1, ξ_2)

A parametric study is undertaken to analyze the influence of ξ_1 and ξ_2 on the modal damping. The amplitude of motion of the elastomer is fixed at 0.00015. Results are obtained for various values of ξ_1 keeping ξ_2 fixed at 0.25. Figure 16 shows the results for four different values of ξ_1 (0.1, 0.07, 0.04, and 0.02). As ξ_l is reduced, the

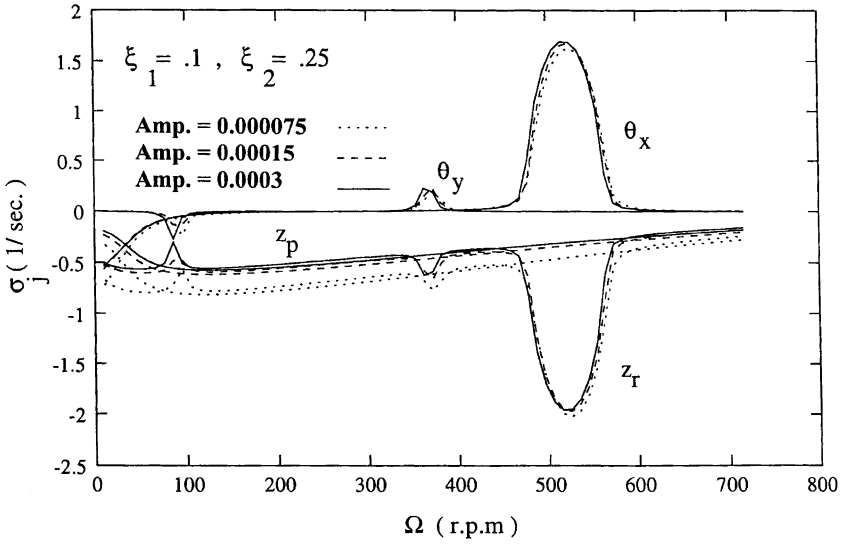

Fig. 15 Effect of amplitude of motion of elastomer on modal damping: $\xi_1 = 0.1$, and $\xi_2 = 0.25$.

maximum levels of instability in roll θ_x (rpm range 480–620) and pitch θ_y (rpm range 350–420) are reduced. The region of instability is also shifted to a higher rpm range. The reason for the shift can be attributed to the increase in lag frequencies as ξ_l is reduced. The progressive Z_p and regressive Z_r lag damping significantly increases with reduction in ξ_1.

Next, the influence of ξ_2 on the ground resonance stability is studied by varying the value of ξ_2 while keeping ξ_1 fixed. Figure 17 shows the variation of the modal damping for three different values of ξ_2 (namely, 0.15, 0.23, and 0.35) while ξ_l is fixed at 0.04. It is observed that for the combination $\xi_1 = 0.04$ and $\xi_2 = 0.23$ the levels of instability in pitch θ_y and roll θ_x modes are minimum. Also, for this combination, progressive and regressive lag modes have high value of damping. This observation clearly indicates that for a given value of ξ_1 there is a particular value of ξ_2 for which the level of instability is minimum. To highlight this observation, the stability analysis is performed by varying the values of ξ_1 from 0.01 to 0.1 in steps of 0.01 and that of ξ_2 from 0.15 to 0.35 in steps of 0.01. The variation of damping in roll mode corresponding to the maximum instability is shown in a three-dimensional plot (Fig. 18). This figure clearly shows that the roll damping exhibits a convex shape with a distinct minimum with respect to ξ_2. The reason for this interesting observation is that the elastomer deformation is dependent on the relative displacement between the torque tube and the flex beam, which is dependent on the mode shape of lag motion. For a certain combination of $\xi_1$and ξ_2, the elastomer deformation results in providing a maximum value of damping to the system. Therefore, by a judicial selection of the locations of the elastomer and torque tube the stability of the system can be enhanced taking into account the fatigue characteristics of the elastomer.

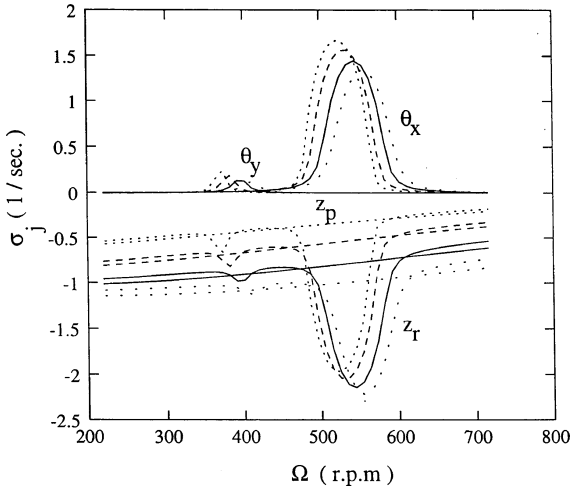

Fig. 16 Modal damping for different locations ξ_1 of the elastomer (zero support damping): ....., $\xi_1 = 0.1, \xi_2 = 0.25$; – – –, $\xi_1 = 0.07, \xi_2 = 0.25$; ——, $\xi_1 = 0.04, \xi_2 = 0.25$; and . . . ., $\xi_1 = 0.02, \xi_2 = 0.25$.

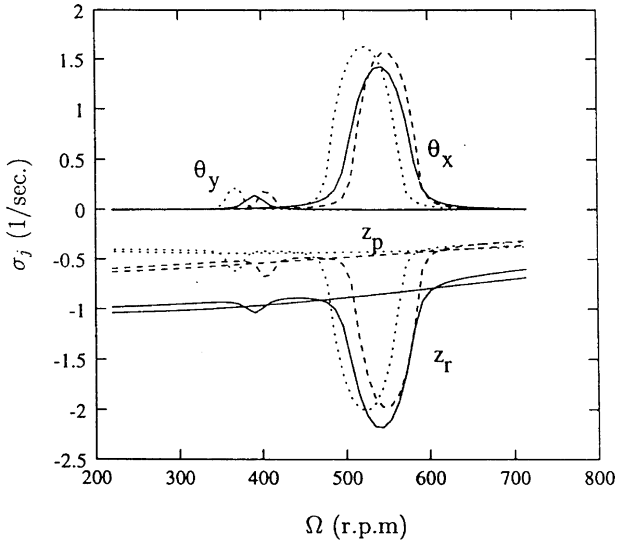

Fig. 17 Modal damping for different locations ξ_2 of the torque tube attachment (zero support damping): ....., $\xi_1 = 0.04$, $\xi_2 = 0.15$; ——, $\xi_1 = 0.04, \xi_2 = 0.23$; and – – –, $\xi_1 = 0.04, \xi_2 = 0.35$.

Effect of Support Damper

The analysis is carried out for the configuration ($\xi_1 = 0.1$, $\xi_2 = 0.25$). The damping ratios in the pitch and roll modes are assumed to be $\xi_{\theta_y} = 0.0529$ and $\xi_{\theta_x} = 0.082$. The amplitude of elastomer motion is taken as 0.00015. Figure 19 shows that for the baseline configuration with zero support damping the level of instability in the roll mode θ_x is $\sigma = 1.67\ s^{-1}$ in the speed range of 440–600 rpm. With the inclusion of support damper, the maximum level of instability in roll mode is brought down to $0.87\ s^{-1}$. But the region of instability spreads over a wider range of operating speeds (470–640 rpm). To highlight the importance of elastomer location on stability, the results corresponding to another configuration ($\xi_1 = 0.04, \xi_2 = 0.25$) are also shown in Fig. 19. With support damping, this configuration has a maximum level of instability of $0.53\ s^{-1}$ in roll mode, which is lower than that of the baseline configuration. The region of instability is also reduced to 515–580 rpm.

Keeping the other parameters the same, when the support damping in the roll mode is further increased to $\zeta_{\theta_y} = 0.20$ the configuration ($\xi_1 = 0.04, \xi_2 = 0.25$) becomes stable for the entire range of rotational speeds, whereas the configuration ($\xi_1 = 0.1, \xi_2 = 0.25$) is unstable beyond 475 rpm, as shown in Fig. 20.

These results indicate that inclusion of the support damper reduces the level of the instability considerably. In addition, for a given value of fuselage damping, a proper choice of elastomer location can improve the stability of the system over the entire rpm range.

Response Analysis in Time Domain

A detailed time response analysis of the coupled rotor/fuselage dynamic system to a given initial disturbance is carried out to

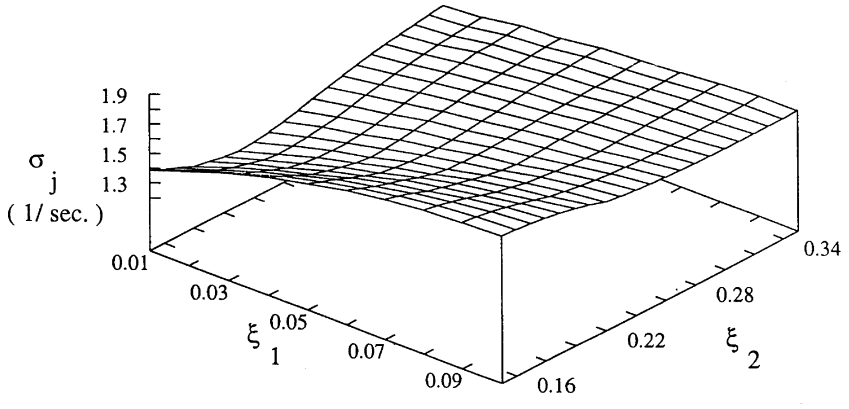

Fig. 18 Variation of maximum instability in roll mode for different combination of ξ_1 and ξ_2.

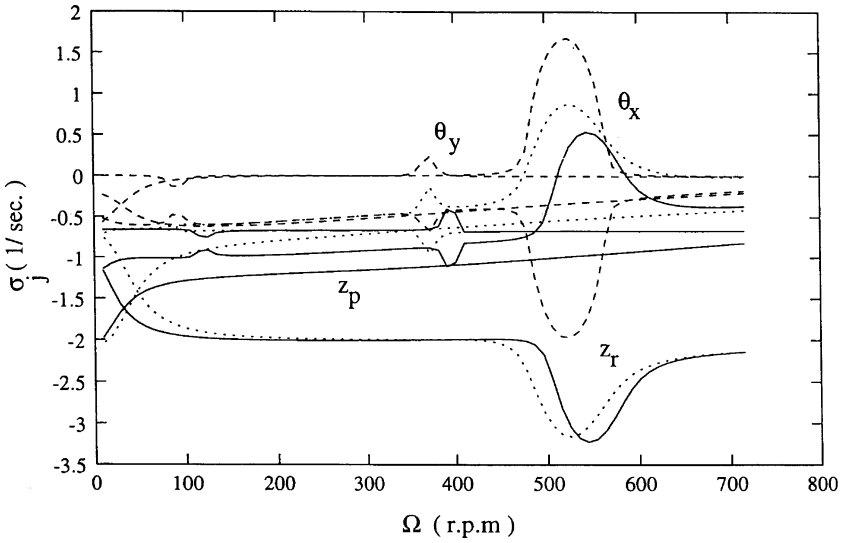

Fig. 19 Effect of support damping on stability ($\zeta_{\theta_x} = 0.082$, $\zeta_{\theta_y} = 0.0529$): – – –, no support damping ($\xi_1 = 0.1$, $\xi_2 = 0.25$) baseline configuration; ....., with support damping ($\xi_1 = 0.1$, $\xi_2 = 0.25$); and ——, with support damping ($\xi_1 = 0.04$, $\xi_2 = 0.25$).

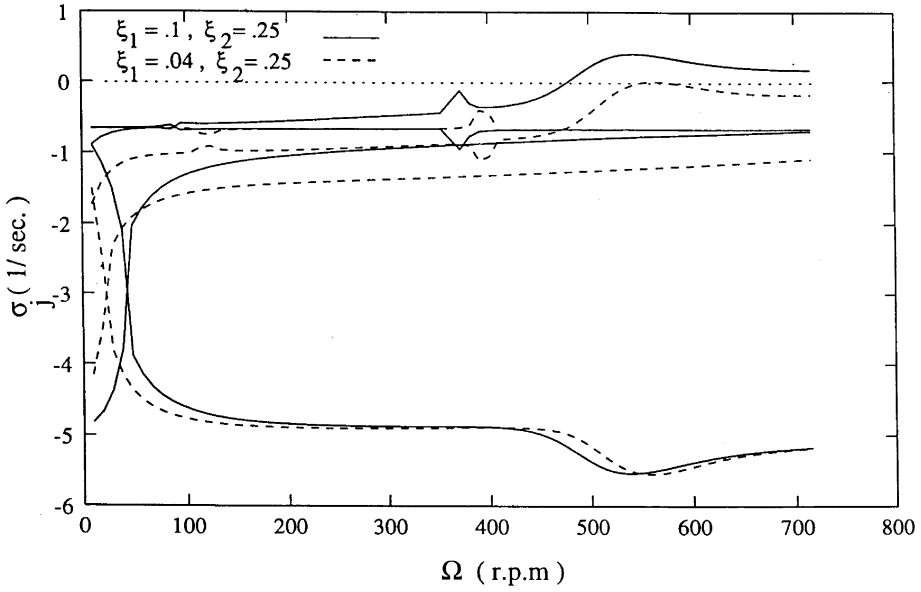

Fig. 20 Effect of support damping on stability ($\zeta_{\theta x} = 0.20$, $\zeta_{\theta y} = 0.0529$): ——, $\xi_1 = 0.1$, $\xi_2 = 0.25$; and – – –, $\xi_1 = 0.04$, $\xi_2 = 0.25$.

examine the stability behavior of the system in time domain. For the baseline configuration, the locations of the elastomer and torque tube are taken as $\xi_1 = 0.1$ and $\xi_2 = 0.25$, respectively. The damping ratios in pitch and roll modes are $\zeta_{\theta_x} = 0.082$ and $\zeta_{\theta_y} = 0.0529$, respectively. (For this configuration, the rpm range of instability of the system identified by the linearized eigenanalysis is 470–640 rpm, as shown in Fig. 19).

The results are generated for a wide range of rotor rpm and initial disturbance in roll mode. The rpm range is 250 to 700 rpm. The initial disturbance in roll mode is varied in the range $\theta_x(0) = 0.1$ to 10.0 degrees. The initial conditions corresponding to other degrees of freedom are taken as zero, for all of the cases. For the sake of conciseness, results pertaining to a few cases are presented next.

At 450 rpm, an initial disturbance of $\theta_x(0) = 0.8$ deg is applied. The corresponding time response of the individual blade and fuselage degrees of freedom are shown in Figs. 21a and 21b. Figures 22a and 22b show the time response of the system for an initial disturbance of $\theta_x(0) = 4.0$ deg. In Figs. 21 and 22, it can be noted that to highlight the response of the blades and fuselage pitch motion a suitable scale is used, which is much smaller than the one used for the roll motion. It is evident that the time response indicates a stable system for both the cases. On the other hand, under the same operating condition for an initial disturbance of $\theta_x(0) = 10.0$ deg, it is observed that the time response in all degrees of freedom show a diverging behavior indicating that the system is unstable (Figs. 23a and 23b).

Based on the convergence/divergence criteria of the time response, the region of instability as a function of rotor rpm and initial disturbance in θ_x has been identified. This region is presented in the form of a two-dimensional plot as shown in Fig. 24. It can be observed that the region of instability is a function of amplitude of initial disturbance and also that the rpm range of instability increases with the increase in amplitude of disturbance. For comparison, the rpm range of instability obtained from eigenanalysis of linearized equations is also shown in Fig. 24 by the dashed lines. In the case of eigenanalysis, the rpm range of instability of the system is 470–640 rpm. It can be seen that even though the rpm range of instability predicted by the eigenanalysis and time response calculation lie in the same neighborhood the stability boundary seems to differ considerably, indicating the effect of magnitude of initial disturbance on the ground resonance stability.

To delineate the effect of nonlinearities of the elastomer on the stability of the system, a time-domain analysis is carried out after neglecting all of the nonlinear terms associated with the elastomer

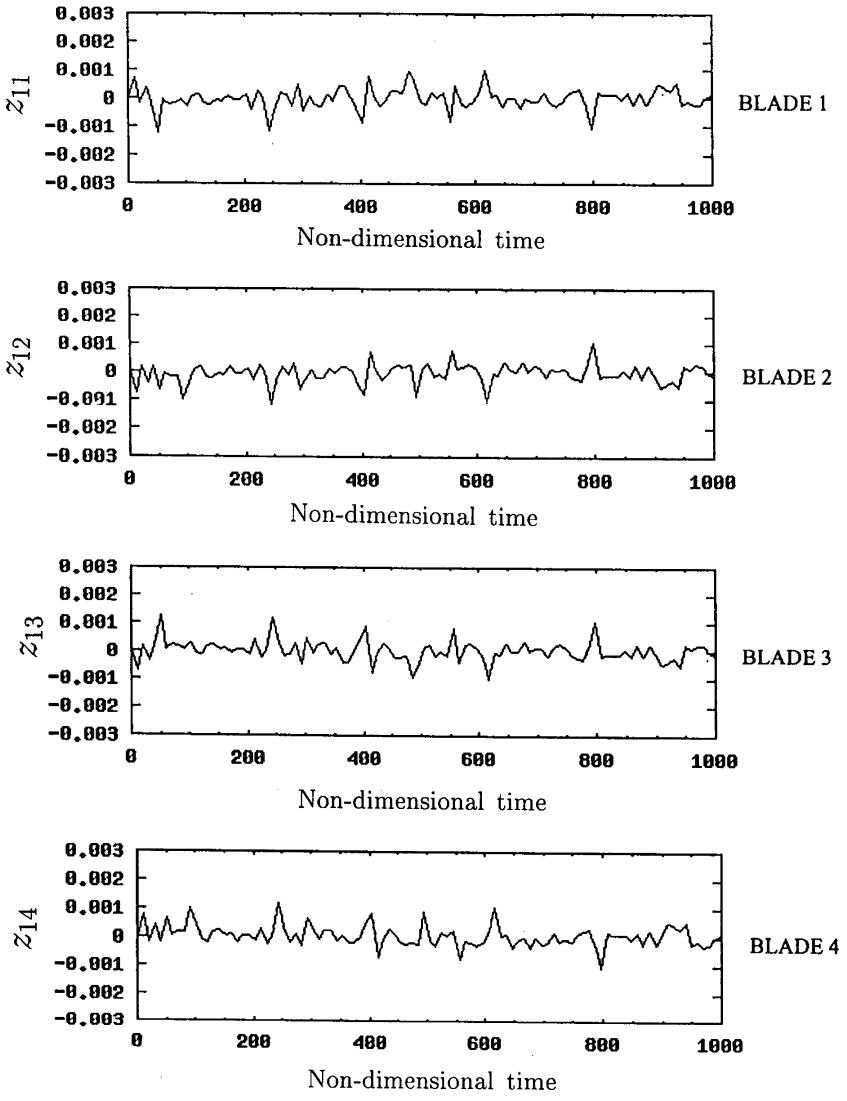

Fig. 21a Blade motion in nondimensional time domain: 450 rpm, $\theta_x(0) = 0.8$ deg, $\zeta_{\theta_x} = 0.082$, and $\zeta_{\theta_y} = 0.0529$.

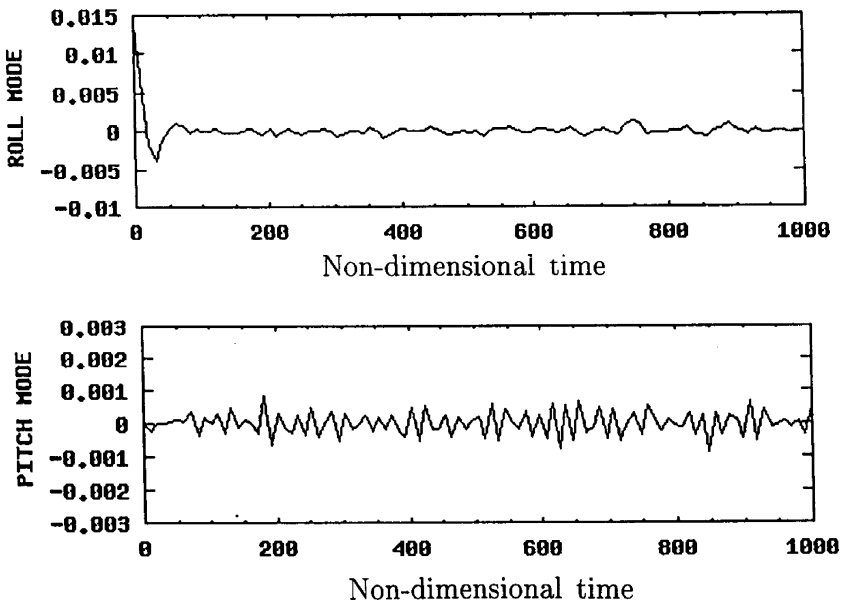

Fig. 21b Fuselage motion in nondimensional time domain: 450 rpm, $\theta_x(0) = 0.8$ deg, $\zeta_{\theta_x} = 0.082$, and $\zeta_{\theta_y} = 0.0529$.

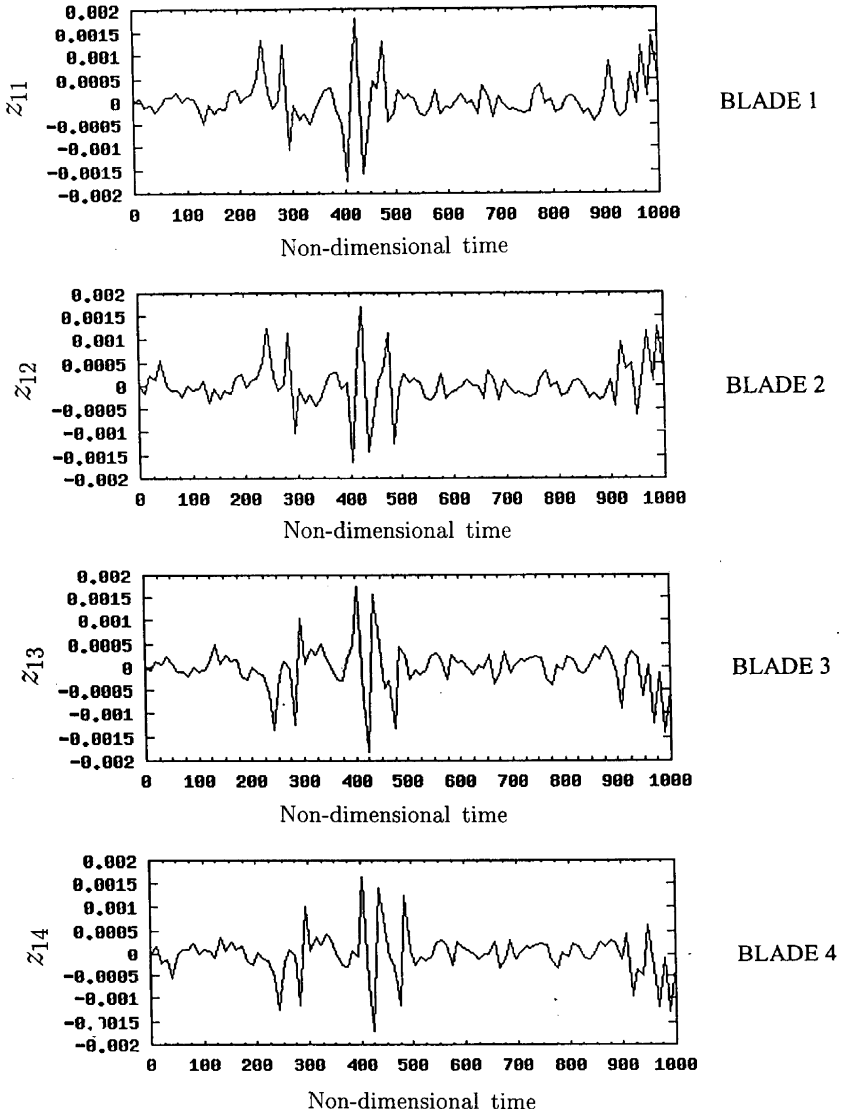

Fig. 22a Blade motion in nondimensional time domain: 450 rpm, $\theta_x(0) = 4$ deg, $\zeta_{\theta_x} = 0.082$, and $\zeta_{\theta_y} = 0.0529$.

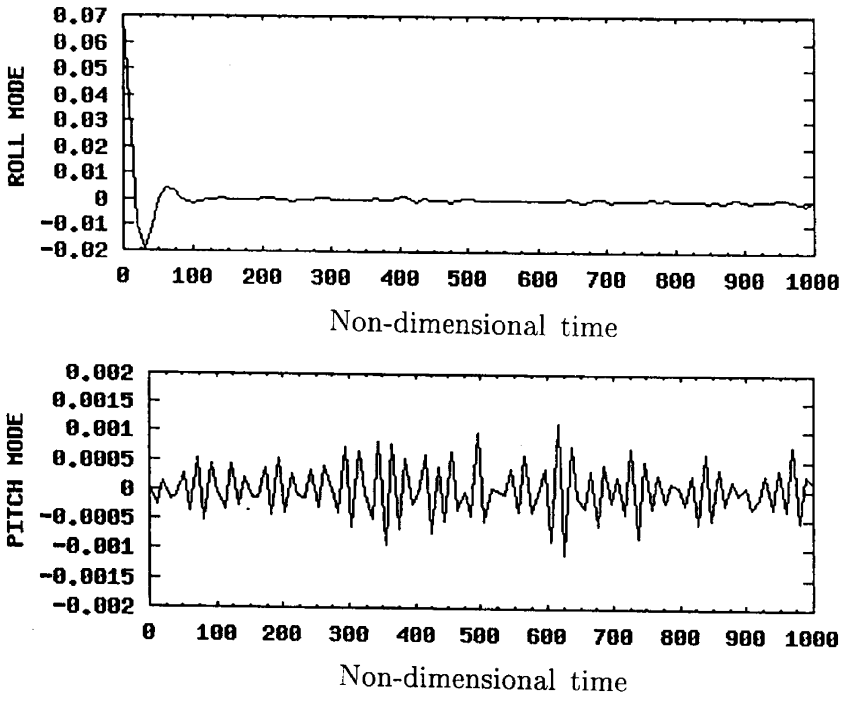

Fig. 22b Fuselage motion in nondimensional time domain: 450 rpm, $\theta_x(0) = 4$ deg, $\zeta_{\theta_x} = 0.082$, and $\zeta_{\theta_y} = 0.0529$.

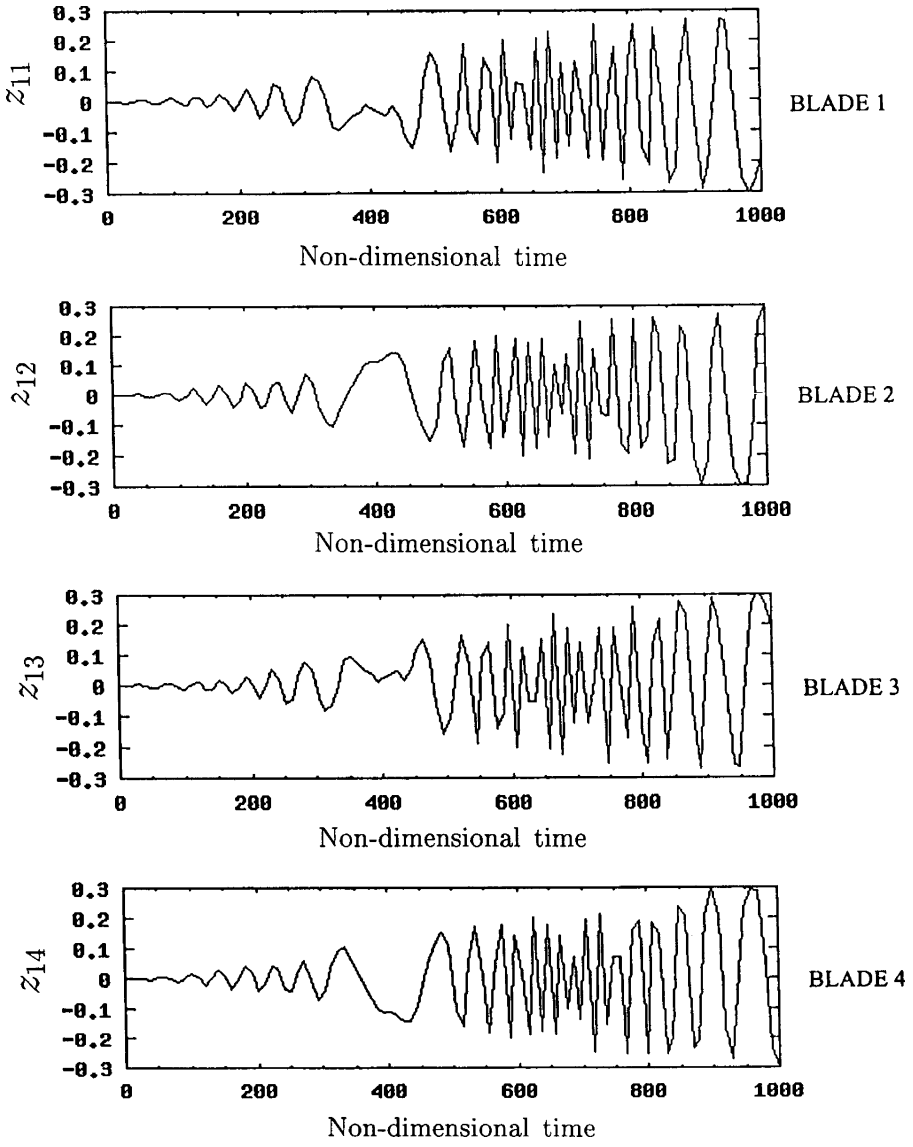

Fig. 23a Blade motion in nondimensional time domain: 450 rpm, $\theta_x(0) = 10$ deg, $\zeta_{\theta_x} = 0.082$, and $\zeta_{\theta_y} = 0.0529$.

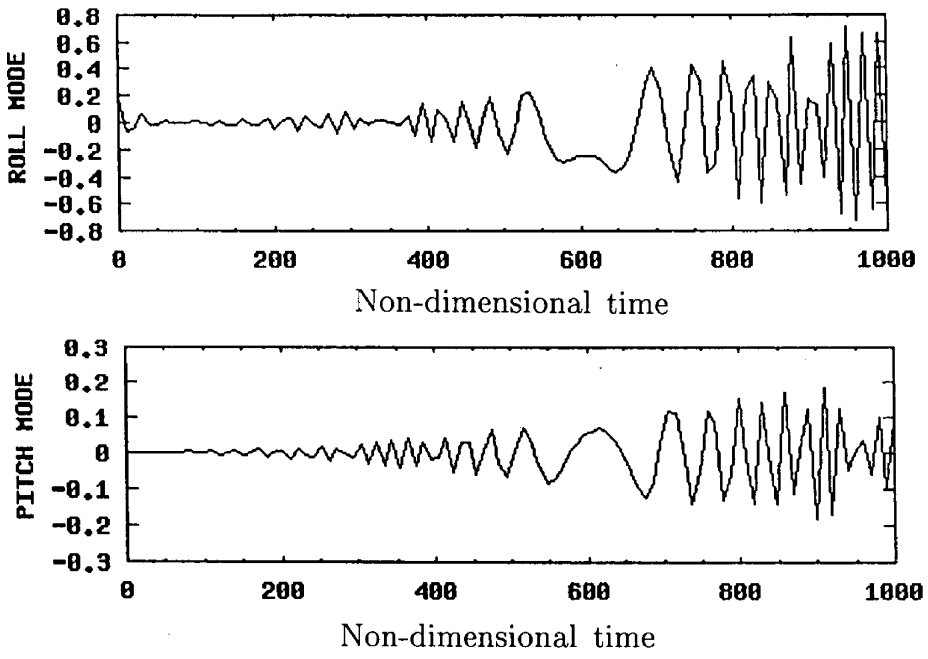

Fig. 23b Fuselage motion in nondimensional time domain: 450 rpm, $\theta_x(0) = 10$ deg, $\zeta_{\theta_x} = 0.082$, and $\zeta_{\theta_y} = 0.0529$.

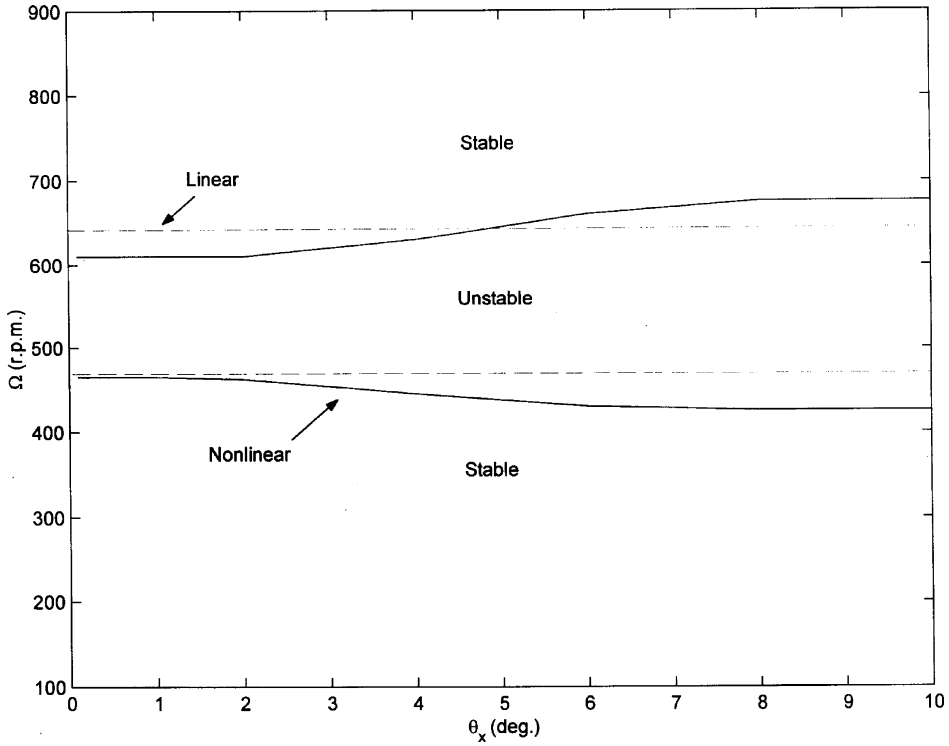

Fig. 24 Stability boundary as a function of rotor rpm and initial disturbance in roll obtained from time response analysis (nonlinear): – – –, stability boundary for eigenanalysis (linear).

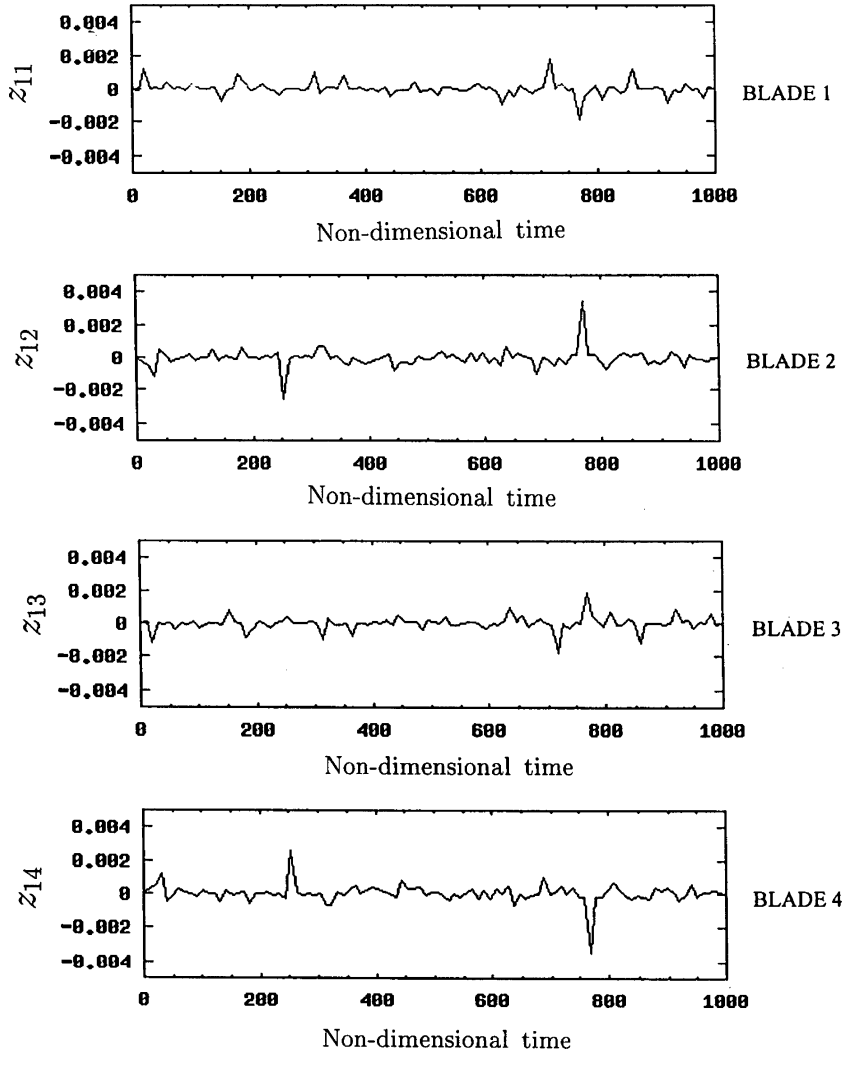

Fig. 25a Blade motion in nondimensional time domain (linear elastomer): 450 rpm, $\theta_x(0) = 10$ deg, $\zeta_{\theta_x} = 0.082$, and $\zeta_{\theta_y} = 0.0529$.

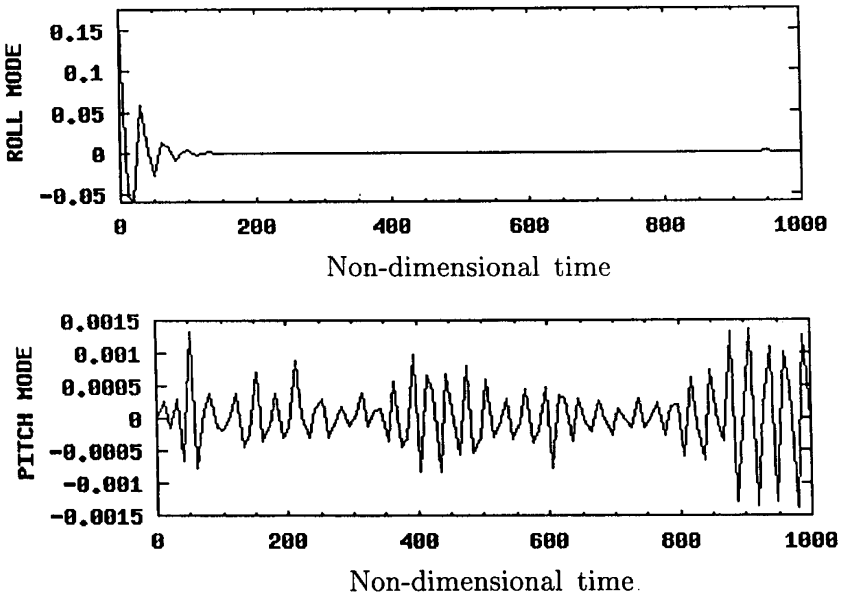

Fig. 25b Fuselage motion in nondimensional time domain (linear elastomer): 450 rpm, $\theta_x(0) = 10$ deg, $\zeta_{\theta_x} = 0.082$, and $\zeta_{\theta_y} = 0.0529$.

[from the nonlinear term $\hat{F}_{\mathrm{NL}}$ of Eq. (22)] but keeping the initial and operating conditions same. The results indicated that the instability of the system in the rotor operation ranges 420–470 rpm and 620–700 rpm is entirely caused by elastomer nonlinearity. One illustrative set of results corresponding to the operating rpm of 450, and initial disturbance of $\theta_x(0) = 10.0$ deg is presented in Figs. 25a and 25b. For this case, the response of the system shows a stable condition. On the other hand, under the same operating and initial conditions, time response of the system with nonlinear elastomer indicates unstable behavior (Figs. 23a and 23b). However, in the range 470–620 rpm both linear and nonlinear elastomer models showed diverging time response indicating instability of the system. The linearised eigenanalysis also predicted instability of the system in the range 470–620 rpm.

Conclusions

The highly nonlinear viscoelastic characteristics of an elastomeric damper are modeled by a parallel combination of spring and damper elements. The stiffness and damping parameters of the model are identified from a set of experimental data taken from the literature.

Nonlinear free vibration of the rotating blade under lag bending has been studied. A numerical perturbation technique is applied to determine the frequency-amplitude relationship. It is concluded that up to a fairly high value of amplitude a seventh-order approximation for the restoring force is sufficient to correctly predict the frequency-amplitude relationship. The alternating sign in the polynomial expressing the restoring force prevents the nonlinear frequency-amplitude relation to be monotonically softening or hardening.

The ground resonance stability of the coupled rotor-body system has been carried out by two approaches, namely, eigenanalysis of linearized equations with amplitude-dependent coefficients and direct time reponse analysis of nonlinear equations to an initial disturbance.

The results of the linearized eigenanalysis indicate that the amplitude of elastomer motion does not significantly alter the stability of the system in the region of maximum instabilities. It is observed that the modal damping of the progressive lag mode decreases appreciably with increasing amplitude.

The locations of the elastomer and torque tube attachment seem to have significant influence on the stability of the system. The results indicate that for a given location of the elastomer there is an optimum location for the torque tube providing least instability in the system. Therefore, a judicious selection of the locations of the elastomer and torque tube is very important for enhancing the stability of the system under ground resonance condition.

The time response analysis of the nonlinear equations clearly indicates that the stability of the system is dependent on the amplitude of initial disturbance and it is caused by the nonlinearity of the elastomer. Even though the rpm range of instability predicted by time-domain analysis and eigenanalysis is in the same neighborhood, there is considerable difference in the stability boundary prediced by the two methods, indicating the effect of elastomer nonlinearity on the ground resonance stability of the system.

Acknowledgment

The authors wish to acknowledge the financial support from the Structures Panel of the Aeronautics Research and Development Board, India.

The authors thank M. Srivastava for his assistance in computation.

References

[1]Hodges, D. H., "A Theoretical Technique for Analyzing Aeroelastic Stability of Bearingless Rotors," *AIAA Journal*, Vol. 17, No. 4, 1978, pp. 400–407.

[2]Hodges, D. H., "An Aeromechanical Stability Analysis for Bearingless Rotor Helicopters," *Journal of the American Helicopter Society*, Vol. 24, No. 1, 1979, pp. 2–9.

[3]Sivaneri, N. T., and Chopra, I., "Finite Element Analysis for Bearingless Rotor Blade Aeroe-Lasticity," *Journal of the American Helicopter Society*, Vol. 29, No. 2, 1984, pp. 42–51.

[4]Dull, A. L., and Chopra, I., "Aeroelastic Stability of Bearingless Rotors in Forward Flight," *Journal of the American Helicopter Society*, Vol. 33, No. 4, 1988, pp. 38–46.

[5]Jang, J., and Chopra, I., "Ground and Air Resonance of an Advanced Bearingless Rotor in Hover," *Journal of the American Helicopter Society*, Vol. 33, No. 3, 1988, pp. 20–29.

[6]Gandhi, F., and Chopra, I., "An Analytical Model for a Nonlinear Elastomeric Lag Damper and Its Effect on Aeromechanical Stability in Hover," *Journal of the American Helicopter Society*, Vol. 39, No. 4, 1994, pp. 59–69.

[7]Gandhi, F., and Chopra, I., "Analysis of Bearingless Main Rotor Dynamics with the Inclusion of an Improved Time Domain Nonlinear Elastomeric Damper Model," *Journal of the American Helicopter Society*, Vol. 41, No. 3, 1996, pp. 267–277.

[8]Panda, B., and Mychalowycz, E., "Aeroelastic Stability Wind Tunnel Testing with Analytical Correlation of the Comanche Bearingless Main Rotor," *Journal of the American Helicopter Society*, Vol. 42, No. 3, 1997, pp. 207–217.

[9]Ormiston, R. A., Saberi, H., and Anastassiades, T., "Application of 2GCHAS to the Investigation of Aeromechanical Stability of Hingeless Rotor Helicopters," *Proceedings of the 51st Forum of the American Helicopter Society*, American Helicopter Society, Alexandria, VA, 1995, pp. 1132–1155.

[10]Mallik, A. K., Kher, V., Puri, M., and Hatwal, H., "On the Modelling of Nonlinear Elastometic Vibration Isolators," *Journal of Sound and Vibration*, Vol. 219, No. 2, 1999, pp. 239–253.

[11]Gobel, E. F., *Rubber Springs Design*, Newnes-Butterworths, London, 1974, Chap. 1.

[12]Wereley, N. M., Snyder, R., Krishnan, R., and Sieg, T., "Helicopter Damping," *Encyclopedia of Vibration*, edited by D. Ewins and S. S. Rao, Academic Press, New York, 2001, pp. 629–642.

[13]McGuire, D. P., "The Application of Elastomeric Lead-lag Dampers to Helicopter Rotors," Lord Library, Technical Papers No. LL2133, Erie, PA, 1976.

[14]Hausmann, G., "Structural Analysis and Design Considerations of Elastomeric Dampers with Viscoelastic Material Behavior," *Twelfth European Rotorcraft Forum*, Garmisch-Partekirchen, Germany, Sept. 1986, pp. 70.1–70.26.

[15]Felker, F., Lau, B., McLaughlin, S., and Johnson, W.,"Nonlinear Behavior of an Elastomeric Lag Damper Undergoing Dual-frequency Motion and Its Effect on Rotor Dynamics," *Journal of the American Helicopter Society*, Vol. 34, No. 4, 1987, pp. 45–53.

[16]Kunz, D. L.,"Influence of Elastomeric Damper Modeling on the Dynamic Response of Helicopter Rotors," *AIAA Journal*, Vol. 35, No. 2, 1997, pp. 349–354.

[17]Lesieutre, G. A., and Bianchini, E., "Time-Domain Modeling of Linear Visco-Elasticity Using Anelastic Displacement Fields," *Journal of Vibration and Accoustics*, Vol. 117, No. 4, 1995, pp. 424–430.

[18]Smith, E. C., Beale, M. R., Govindswamy, K., Vascsineci, M. J., and Lesieutre, G. A., "Formulation and Validation of a Finite Element Model for Elastomeric Lag Dampers," *Proceedings of the 51st Annual Forum of the American Helicopter Society*, American Helicopter Society, Alexandria, VA, 1995, pp. 1101–1116.

[19]Govindswamy, K., Smith, E. C., and Lesieutre, G. A., "Aero-Thermoelastic Behavior of Helicopter with Elastomeric Lag Dampers," *Proceedings of the American Helicopter Society Aeromechanics Specialists' Meeting*, American Helicopter Society, Alexandria, VA, 1995, pp. 8.52–8.70.

[20]Brackbill, C. R., Lesieutre, G. A., Smith, E. C., and Govindswamy, K., "Thermo Mechanical Modeling of Elastomeric Materials," *Journal of Smart Materials and Structures*, Vol. 5, No. 5, 1996, pp. 529–539.

[21]Byers, L. K., Lesieutre, G. A., Smith, E. C., and Beale, M. R., "Transient Behavior of Elastomeric Damper and Bearing Materials," AIAA Paper 96-1218, April 1996.

[22]Ruhl, L. E., Lesieutre, G. A., Brackbill, C. R., and Smith, E. C., " Thermomechanical Modeling of Elastomeric Damper Materials," AIAA Paper 99-1221, April 1999.

[23]Brackbill, C. R., Lesieutre, G. A., Ruhl, L. E., and Smith, E. C., "Characterization and Modeling of the Low Strain Amplitude and Frequency Dependent Behavior of Elastomeric Damper Materials," AIAA Paper 98-1845, April 1998.

[24]Gandhi, F., and Chopra, I., "A Time Domain Non-Linear Viscoelastic Damper Model," *Journal of Smart Materials and Structures*, Vol. 5, 1996, pp. 517–528.

[25]Potter, J. L., McGuire, D. P., and Brubaker, E. L., "Elastomers + Fluid + Electronics = Improved Comfort and Reliability for Aircraft," *Proceedings of the International Exhibition Cum Seminar on Helicopter Development and Utilisation in South Asia-Pacific*, Aeronautical Society of India, Bangalore, India, Oct. 1995, pp. 6.3-1–6.3-19.

[26]Bagley, R. L., and Torvik, P. J., "A Theoretical Basis for the Application of Fractional Calculus to Viscoelasticity," *Journal of Rheology*, Vol. 27, No. 3, 1983, pp. 201–210.

[27]Pohit, G., Mallik, A. K., and Venkatesan, C., "Free Out-Of-Plane Vibration of a Rotating Beam with Non-Linear Elastomeric Constraints," *Journal of Sound and Vibration*, Vol. 220, No. 1, 1999, pp. 1–25.

[28]Pohit, G., "Dynamics of a Bearingless Helicopter Rotor Blade with a Non-Linear Elastomeric Constraint," Ph.D Dissertation, Dept. of Mechanical Engineering, Indian Inst. of Technology, Kanpur, India, Feb. 1999.

[29]Pakdemirli, M., and Nayfeh, A. H., "Nonlinear Vibration of a Beam-Spring-Mass System," *Journal of Vibration and Acoustics*, Vol. 116, No. 4, 1994, pp. 433–439.